In situ observations of crack propagation mechanisms along interfaces between confined polymer layers and glass

Vellinga, W. P.; van Tijum, R.; De Hosson, J. Th. M.

Published in:
Applied Physics Letters

DOI:
10.1063/1.2172713

In situ observations of crack propagation mechanisms along interfaces between confined polymer layers and glass

W. P. Vellinga, R. Timmerman, R. van Tijum, and J. Th. M. De Hosson
Department of Applied Physics, Materials Science Centre and The Netherlands Institute for Metals Research, University of Groningen, Nijenborgh 4, 9747 AG Groningen, The Netherlands

(Received 15 August 2005; accepted 11 January 2006; published online 9 February 2006)

This paper concentrates on microscopic observations of the propagation of cracks along polymer-glass interfaces and crack propagation mechanisms. The experimental set-up consists of an asymmetric double cantilever beam in an optical microscope. Image processing techniques used to isolate the crack fronts are presented. The fronts propagate inhomogeneously in space and time, i.e., in bursts that spread laterally along the front over a certain distance. It is interesting to note that two different cases are detected; one in which crack propagation is dominated by initiation of instabilities on the front, and another one in which it is dominated by propagation of existing instabilities. © *2006 American Institute of Physics*. [DOI: 10.1063/1.2172713]

Polymer-metal interfaces appear in an ever-increasing number of applications, as diverse as car panels and high-tech displays. The mechanical integrity of the interface in such applications is important and as a consequence the precise propagation of a crack along it is a challenging objective for investigation. There is growing interest in bringing together theory on crack propagation from continuum mechanics with ideas from statistical physics on the effects of disorder. This may prove in particular helpful for lifetime prediction where quantities accessible from continuum mechanics (stresses, stress intensity factors, energy release rates) may be related to the interplay between disorder and stress-aided thermally activated processes.[1] In crack initiation and propagation locally stored elastic energy is released through the formation of a crack surface, generation of heat, and possibly associated irreversible plastic deformation. This means that local fluctuations in geometry, e.g. layer thickness, interface bonding or material properties may contribute to disorder in the local toughness or energy release rate associated with the interface crack. Recently, experiments on cracks propagating along weak PS-PS interfaces have revealed scaling behavior of crack front shape and crack front dynamics.[2,3] The degree of disorder, local stress concentrations near irregularities on the front, or elastic interaction (potentially long range) along the front are all expected to influence the crack shape and crack dynamics (for a review, see, e.g., Ref. 4). In this respect an analogy may exist with the formation of patterns of channeling cracks in disordered brittle layers on a ductile or elastic substrate. For such patterns it has been established that the stress amplification near a crack-tip favors crack propagation and that for large enough stress amplification a crack, once nucleated, will propagate over the length of the sample. In contrast, if stress amplification is very small nucleation on sites determined by the quenched disorder is favored and the propagation of the resulting cracks is limited by the screening of the external field by already existing cracks.[5]

We present new microscopic observations on the propagation of cracks along polymer-glass interfaces and focus on the method of analysis as well as on propagation mechanisms. The experimental method is an Asymmetric Double Cantilever Beam (ADCB) test. The actual setup is based on a miniature tensile stage, which fits in a reflection optical microscope. Driving speeds for the cracks are typically 10 μm/s. Samples consist of glassy polyethylene terephthalate (PETG) spin-coated on steel, with a thickness of 15 μm, dried in a convection oven at 80 °C for a few hours, and subsequently pressure bonded to a glass support (for 240 s, at 140 °C and 1.5 MPa). For a schematic picture of the experiment see Fig. 1. In the experiment a crack may propagate along the PET-glass interface as well as along the rough and anisotropic PET-steel interface (rms $\sim$ 1 μm). Here we only show results of propagation along the PET-glass interface whereas results for the PET-steel interface will be reported elsewhere. The crack front is observed through the glass with a CCD camera (1376 $\times$ 1032 pixels, 3 $\times$ 8 bit) at a rate of 1 Hz.

In ADCB experiments one deals with the geometry shown in Fig. 1. For details on ADCB experiments and related issues reference is made to Ref. 6. In practice $a \gg h_1$, h_2. Also at all times, for the remaining adhered portion of the beam L, $L \gg a$ should hold. In ADCB we measure the energy release rate for a certain interface structure, sample geometry and phase angle by measuring a as shown in Fig. 1 and using the approximate formulae shown below,[6]

$$G = \frac{(3\Delta^2 E_1 E_2 h_1^3 h_2^3)(C_2^2 E_1 h_1^3 + C_1^2 E_2 h_2^3)}{8a^4 \Lambda^2} \tag{1}$$

with $\Lambda = C_1^3 E_2 h_2^3 + C_2^3 E_1 h_1^3$ and $C_i = 1 + 0.64 h_i / a$. A typical unprocessed image of a crack front is shown in Fig. 2(a1).

In the experiment the position of the knife is fixed, and the sample is clamped in one of the clamps of the tensile stage. The movement of the clamps may not be entirely

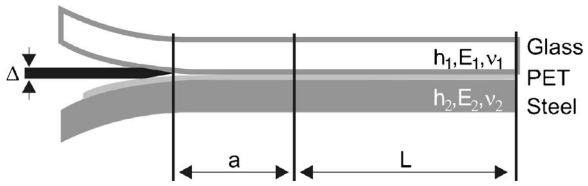

FIG. 1. Schematic drawing of an ADCB experiment. A razor blade (black) is inserted between PET and glass. Δ, crack opening; a, crack length; L, uncracked length. h_i, height; E_i, Young's modulus; ν_i, Poisson's ratio; subscript $i = 1, 2$ refer to glass, steel, respectively.

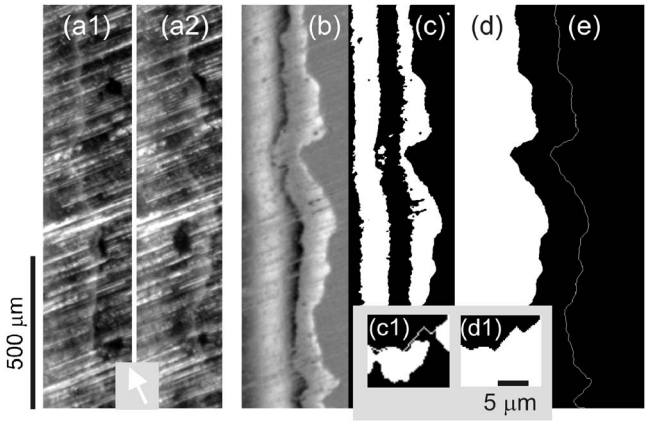

FIG. 2. Front 1. (a1) Part of image I_0 at t_0, showing metal roughness, wedge fringes where laminate has separated (left), brightness change at crack front. (a2) Part of image I_{30} at t_0+30 (s). Arrow represents exaggerated displacement vector necessary to bring background into registry. (b) Pixelwise subtraction $I_{30}-I_0$ after image registration. (c) Thresholding. (d) Filling behind front. (e) Front. Insets: Example of treatment of holes. (c1) Type 2 hole in some image I_{i+1} combined with front from I_i. (d1) $C_{i+1}=OR(T_{i+1},C_i)$.

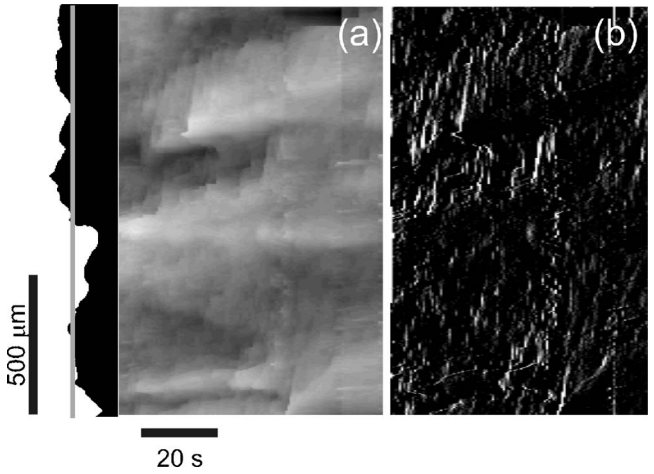

FIG. 3. (a) Example of front 1. Grey line indicates the mean front position $\bar{x}$. (b) $\Delta x_i(t)=x_i(t)-\bar{x}(t)$, light parts: $x_i(t)>\bar{x}(t)$, dark parts: $x_i(t)<\bar{x}(t)$. (c) Forward "acceleration" $\Delta x(t)/\Delta t$ [with $\Delta t=1$ (s)] as a function of time and position along front. $G=2$ J/m^2.

smooth, or aligned with the coordinate system of the image. Image correlation allows determination of the movement of the sample between two images, and subsequently the movement of the front with respect to the sample during the same time can be determined. The translation vector between two images I_i and I_j is indicated by the position of the maximum of the phase correlation function

$$\mathbf{x}(I_i,I_j)=\max\left(F^{-1}\left(\frac{F(I_i)F(I_j)^*}{|F(I_i)F(I_j)^*|}\right)\right), \tag{2}$$

where F in Eq. (2) denotes the discrete Fourier transform. For these experiments I_i and I_j were subimages of 512 $\times$512 pixels ahead of the moving front. The image series is divided into sets of n images, the first of which are "base" images. The displacement vectors between these base images are first calculated. Subsequently, the displacement vectors between images in a certain set and the base image of the set are calculated. Finally the displacement of a certain image N with respect to the first follows from

$$\mathbf{x}(I_1,I_N)=\sum_{i=1}^{N\backslash n}\mathbf{x}(I_{(i-1)},I_{in})+\mathbf{x}(I_{(N\backslash n)n},I_N), \tag{3}$$

where \ in Eq. (3) denotes integer division. In order to isolate the fronts we subtract two images that are n frames apart. [In Fig. 2, the substraction of Fig. 2(a1) and a shifted version of Fig. 2(a2) gives Fig. 2(b).] If the correlation is good this gets rid of the background effectively as can be seen in Fig. 2(b). The main stages in the determination of the front position are shown in Figs. 2(c)–2(e). The subtraction image is noise filtered and thresholded. This leads to Fig. 2(c) which shows a solid area directly behind the front, the rightmost edge in the figure, as well as one slightly further back (left) that results from the first of the wedge fringes that form behind the front. Subsequently the black areas area to the left of the front are filled, Fig. 2(d), and finally the front is isolated subtracting an eroded version of this image from itself, Fig. 2(e). This is relatively straightforward, but problems occur when the stadium illustrated in Fig. 2 shows holes, which is often the case. Either the front may not have moved in the time between the acquisition of the two images (type 1 hole), or the displacement vector from correlation is in error, which combined with the background texture leads to missing lines (type 2 hole). In either case it is impossible to get to the stage depicted in Fig. 2(d). In the case that type 1 holes exist the front can be reconstructed simply using the positions from the previous front. It was decided to fill type 2 holes in the same way. Typically [see Fig. 2(c1)] these holes are narrow and since together they span only a small fraction of a complete front any other method of filling the holes would only lead to small differences in front geometry. The procedure used is sketched in the inset of Figs. 2(c1) and 2(d1). More precise Fig. 2(d1) arrived as follows: denoting thresholded images [as in Fig. 2(c)] by T and filled images [as in Fig. 2(d)] by C the following is therefore performed in a pixelwise fashion,

$$C_{i+1}=OR(T_{i+1},C_i) \tag{4}$$

and subsequently the area behind the front is filled.

Figures 3–5 show results of experiments carried out on two different laminates. Figure 3 shows results on 1 laminate and Figs. 4 and 5 on another laminate. In both cases the

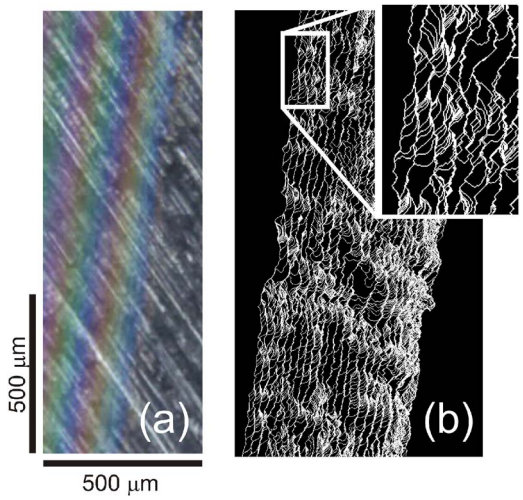

FIG. 4. (a) Snapshot of front 2. (b) Image showing approximately 400 subsequent front positions. Front movement is mainly due to bursts parallel to the front. $G=4$ J/m^2.

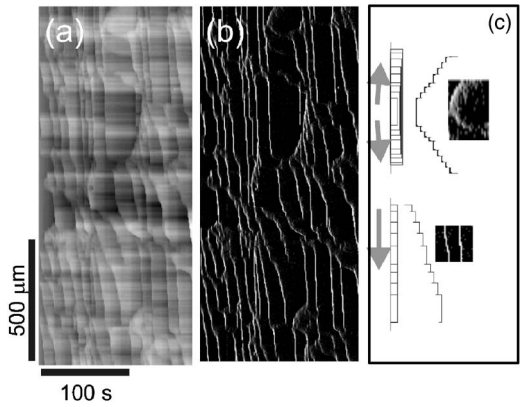

FIG. 5. Propagation of front 2. All displacements with respect to front position at time zero. (a) $\Delta x_i(t) - x_i(0)$. (b) $\Delta x_i(t)/\Delta t$ [with $\Delta t = 1$ (s)]. $G = 4$ J/m^2. (c) Sketches clarifying appearance in (b) of forward bursts (top) and laterally propagating forward steps.

crack was found to propagate essentially along the PET-glass interface. The measured value of G differed slightly between the two laminates, $G = 2$ J/m^2 in the first case, and $G = 4$ J/m^2 in the second case. The front dynamics are displayed in two different ways. Figures 3 and 5 show local front position with respect to the mean front position and local forward acceleration, as a function of time. Figure 4 shows the successive bursts occurring along the crack front. The front shown in Fig. 3 was moving at a constant mean speed of 5 μm/s, the front shown in Figs. 4 and 5 was moving spontaneously (and slowing down) after the knife had been stopped some time before the measurements shown.

The main observation in Figs. 3–5 is that in general the crack propagation is inhomogeneous *in time* as well as *in space*. It is important to realize that although the crack movement is smooth on a macroscopic scale, on a microscopic scale crack movement occurs because parts of the front become unstable and move ahead of the mean crack position.

In Fig. 3 these disturbances are subsequently seen to spread laterally along the front for some distance, with a clear preferred direction, upward in the figure. A qualitatively similar behavior to that shown in Fig. 3 has been found by us for cracks propagating along PET-metal interfaces, and in the literature for polymer-polymer (PS-PS) interfaces.[2,3] This seems to indicate that such crack front movement is in fact quite a common mechanism. In this case weak spatial correlations in the position of the forward bursts can be observed, apparent, e.g., from the directionality in the observed spatiotemporal burst pattern. We speculate that local differences in the energy release rate related to the thickness differences associated with the ridges is responsible for these weak correlations, and for the preferred direction in the burst movement.

Figure 4 shows an essentially similar but more extreme mode of crack propagation. In this case the lateral movement associated with a disturbance may span the entire crack front (i.e., the sample width). In such cases the forward movement of a crack front in fact consists almost entirely of lateral movement of forward steps along the front, a mechanism that is similar to double-kink motion of dislocations in bcc metals. From Fig. 5(b), it is clear that apart from the lateral movement forward bursts do also occur, and that there exists a strong spatial correlation between the position of a burst with that of a subsequent burst. So indeed, an analogy with the formation of crack patterns in supported brittle layers different appears to exist. Interface crack propagation may be dominated by the progression (parallel to and spanning the entire front) of an already existing instability (in this case a double-kinklike protrusion of the front) or by the nucleation of protrusions that move only part of the front forward. In the latter case a correlation with the quenched disorder of the energy release rate is apparent.

Another remarkable feature of the movement shown in Figs. 4 and 5 is the occurrence of a characteristic forward step size. We note that in the literature arrays of regularly spaced shear bands have been observed in front of cracks propagating along interfaces between glassy polymers[3] which could well be responsible for the characteristic step size. More detailed investigation of this aspect and of the scaling properties of crack front are outside the scope of this paper, and will be discussed elsewhere.

In conclusion, crack fronts along a PET-glass interface were found to propagate inhomogeneously *in space* and *time*. The fronts move in forward bursts that spread laterally along the front. Different regimes of crack propagation were encountered. One in which propagation was "initiation" dominated and showed a correlation with the quenched disorder, in this case presumably thickness differences in the confined layer, and one in which propagation was "propagation" dominated and preferentially occurred on positions of the highest stress concentration. Future research will concentrate on the generality of the encountered propagation phenomenology.

The authors would like to acknowledge financial support by IOP (Project No. IOT 01001) and STW (Project No. GTF.4901).

[1] S. Santucci, L. Vanel, and S. Ciliberto, Phys. Rev. Lett. **93**, 095505 (2004).
[2] J. Schmittbuhl and K. J. Måløy, Phys. Rev. Lett. **78**, 3888 (1997).
[3] K. J. Måløy, J. Schmittbuhl, A. Hansen, and G. G. Batrouni, Int. J. Fract. **121**, 9 (2003).
[4] E. Bouchaud, Surf. Rev. Lett. **10**, 797 (2003).
[5] J. V. Andersen, D. Sornette, and K. T. Leung, Phys. Rev. Lett. **78**, 2140 (1997).
[6] B. Bernard, H. R. Brown, C. J. Hawker, A. J. Kellock, and T. P. Russell, Macromolecules **32**, 6254 (1999).